

Three-Dimensional Unsteady Multi-stage Turbomachinery Simulations using the Harmonic Balance Technique

Arathi K. Gopinath^{*}; Edwin van der Weide[†]; Juan J. Alonso[‡]; Antony Jameson[§]

Stanford University, Stanford, CA 94305-4035

Kivanc Ekici[¶] and Kenneth C. Hall^{||}

Duke University, Durham, NC 27708-0300

In this paper, we propose an extension of the Harmonic Balance method for three-dimensional, unsteady, multi-stage turbomachinery problems modeled by the Unsteady Reynolds-Averaged Navier-Stokes (URANS) equations. This time-domain algorithm simulates the true geometry of the turbomachine (with the exact blade counts) using only one blade passage per blade row, thus leading to drastic savings in both CPU and memory requirements. Modified periodic boundary conditions are applied on the upper and lower boundaries of the single passage in order to account for the lack of a common periodic interval for each blade row. The solution algorithm allows each blade row to resolve a specified set of frequencies in order to obtain the desired computation accuracy; typically, a blade row resolves only the blade passing frequencies of its neighbors. Since every blade row is setup to resolve different frequencies the actual Harmonic Balance solution in each of these blade rows is obtained at different instances in time or time levels. The interaction between blade rows occurs through sliding mesh interfaces in physical time. Space and time interpolation are carried out at these interfaces and can, if not properly treated, introduce aliasing errors that can lead to instabilities. With appropriate resolution of the time interpolation, all instabilities are eliminated. This new procedure is demonstrated using both two-and three dimensional test cases and can be shown to significantly reduce the cost of multi-stage simulations while capturing the dominant unsteadiness in the problem.

I. INTRODUCTION

Modern Computational Fluid Dynamics (CFD) methods have reached a significant level of maturity over the past decades: CFD tools are routinely used to provide significant insights into the most complex engineering problems. Steady-state computations have improved to such an extent that they have become an everyday design tool. The situation is quite different, however, for unsteady flow computations as they typically require long integration times and a significant computational investment.

Turbomachinery flows are naturally unsteady mainly due to the relative motion of rotors and stators and the natural flow instabilities present in tip gaps and secondary flows. Full-scale time-dependent calculations for unsteady turbomachinery flows are still too expensive to be suitable for daily design purposes. One of the reasons for this large cost is the fact that in practical turbomachinery configurations blade counts are chosen such that periodicity (other than the whole annulus) does not occur, thus avoiding resonance. In order to minimize the size of the problem that needs to be computed, various approximations are introduced. All of these approximations can be considered to be different variations of reduced-order models. The effective use

^{*}Doctoral Candidate, AIAA Student Member

[†]Research Associate, AIAA Member

[‡]Professor, Department of Aeronautics and Astronautics, AIAA Member

[§]Thomas V. Jones Professor of Engineering, Department of Aeronautics and Astronautics, AIAA Member

[¶]Research Associate, Department of Mechanical Engineering and Materials Science, AIAA Member

^{||}Julian Francis Abele Professor and Chairman, Department of Mechanical Engineering and Materials Science, Associate Fellow AIAA

of these reduced-order models requires that the engineer / designer be aware of a method's capabilities as well as its limitations.

The key trade-off in the computation of unsteady turbomachinery flows is between the accuracy of the method and the cost or *computational efficiency* with which a solution can be obtained. Highly accurate and well-resolved models tend to be limited by the available computing power, while most reduced-order models usually neglect a significant amount of the physics and are therefore not credible for the evaluation of the performance and heat transfer characteristics of a turbomachine. A balance between these extremes is clearly desirable. In order to include the unsteady effects while keeping the computational requirements reasonable, two types of approximations can be distinguished. The first approach involves rescaling the geometry (typically by altering the blade counts and their chords to maintain solidity) such that periodicity assumptions hold in an azimuthal portion of the domain that is much smaller than the full annulus. A second alternative involves the use of the original geometry but compromises the fidelity of the time integration method.

An accurate way to solve an unsteady nonlinear multi-stage, multi-passage problem is to integrate in time the spatially discretized flow equations. This calculation can be extremely expensive in terms of CPU and memory requirements.¹⁻³ One such numerical method is the Backward Difference Formula (BDF).⁴ This algorithm marches the entire system of equations forward in physical time using an implicit time advancement scheme, until a periodic steady state is reached. For typical high RPM turbomachinery problems, this periodic steady state is arrived at only after 4-6 time periods have passed and the flow transients have been eliminated. For multi-stage machines with more than 2 or 3 stages, this estimate is only a lower bound.

The Time Spectral method⁵ is a high-fidelity time integration method that has shown considerable savings in computational costs when compared with the BDF formulation. This time-domain algorithm, which can only be used for periodic problems, uses a Fourier representation in time and hence solves directly for the periodic state without having to resolve numerical transients (which consume most of the resources in a time-accurate scheme like the BDF.) The algorithm solves the full nonlinear unsteady RANS equations hence resolving all unsteady effects. The number of Fourier modes to be resolved is input from the user: the more modes that are included, the higher the accuracy of the calculation as well as its cost, which scales linearly with increasing number of modes.

Another way of solving these periodic problems is to use *frequency-domain* methods that have been well established for aeroelastic applications.⁶⁻⁹ The flow variables in these methods are decomposed into a time-averaged part and an unsteady part. The unsteady perturbation is cast in complex harmonic form and its amplitude and phase are solved at a given frequency.

Computational costs can be significantly lowered by using reduced-order models. The simplest of them for turbomachinery problems is the mixing-plane approach¹⁰ where all unsteadiness is ignored. The size of the spatial problem is reduced to a single passage in each blade row, and a steady computation is carried out in each row. At the interface between blade rows, a circumferential average of the flow variables is passed to the neighbor: all unsteady interactions are ignored.

The BDF, Time Spectral and Frequency Domain methods do accommodate unsteady interactions but often include other approximations to lower computational costs. The BDF and Time Spectral methods are frequently used in combination with scaled geometries, such that a periodic fraction of the annulus is solved instead of the whole annulus. Frequency Domain methods often linearize the equations if the unsteady variation is assumed to be small with respect to the time-averaged part. The size of the spatial problem is also often contained to a single blade passage per row using phase-lag periodic conditions. These phase-lag conditions have changed their form from the first "direct store" method proposed by Erdos et al.¹¹ through the time-inclination method by Giles,¹² to the Fourier series based "shape correction method" by He.^{13,14} They have been extensively used in turbomachinery analysis codes like MSU-TURBO.¹⁵

Ekici and Hall¹⁶ proposed the Harmonic Balance method to solve the full nonlinear RANS equations for turbomachinery problems. The algorithm was implemented and results were discussed for two-dimensional multi-stage compressors. The distinguishing feature of this reduced-order model (compared with the original Harmonic Balance method¹⁷) is that only a specified set of frequencies (comprising combinations of the neighbor's blade passing frequencies) is resolved in each blade row. Unlike single-stage problems, in multi-stage machinery (each blade row has more than one neighbor), this would amount to resolving frequencies that are not multiples of a single fundamental frequency. At the interface between blade rows, the flow variables are Fourier transformed once in time and once in the circumferential direction. These Fourier coefficients are passed on to the neighboring blade row after non-reflecting boundary conditions^{18,19} are

applied to those frequencies that are not coupled (hence eliminating unwanted spurious frequencies), making this a time-domain/frequency-domain method. The Fourier coefficients are then transformed back to the physical domain in the receiving blade row. Similarly to most frequency domain methods, phase-shifted boundary conditions are applied on a single passage computational grid. The main drawback of this method is that it is difficult to apply it for non-radially matched grids and hence the extension to unstructured grids is not straightforward.

In this paper, a different approach is taken. Similarly to the Harmonic Balance technique proposed by Ekici and Hall,¹⁶ combinations of neighbor's blade passing frequencies are resolved in each blade row and phase-lagged periodic boundary conditions are applied on a single passage per row of the turbomachine. The treatment of the sliding mesh interfaces between blade rows is, however, done purely in the time domain. For general non-matching spatial grids at the interfaces, spatial interpolation is carried out. Furthermore, time interpolation is also necessary because different frequencies are resolved in each blade row that differ from those frequencies (and the consequent time steps/levels) in the neighboring blade rows. Spectral interpolation in the presence of non-linear effects introduces aliasing errors which have to be eliminated in order to stabilize the algorithm. These aliasing effects are eliminated by appropriate choices of the time/frequency resolution. Such aliasing instabilities have been encountered in a similar scenario while coupling two different solvers, the Reynolds-Averaged Navier-Stokes (RANS) and the Large-Eddy Simulations (LES) (which resolve different time and length scales) across an interface between a compressor and a combustor.²⁰

The details of the proposed algorithm, its advantages and limitations are explained in the following sections. Wherever possible, the results are compared to a time-accurate solution and accuracy and cost comparisons are presented. Results are discussed for a three-dimensional viscous single-stage case characterized by a single excitation frequency and a second two-dimensional multi-stage case which accommodates multiple excitation frequencies. The entire procedure is implemented in the Sumb solver which allows its application to arbitrarily complex geometry and mesh configurations and to complex viscous flows with a variety of available turbulence models. The intent of the authors is to continue to expand the knowledge about the proposed reduced-order model and to assess its applicability to both performance and aeroelastic problems in complex, multi-stage turbomachinery.

II. MATHEMATICAL FORMULATION

A. Governing Equations

The Navier-Stokes equations in integral form are given by

$$\int_{\Omega} \frac{\partial \mathbf{w}}{\partial t} dV + \oint_{\partial \Omega} \vec{\mathbf{F}} \cdot \vec{\mathbf{N}} ds = 0,$$

where \mathbf{w} is the set of conservative variables and $\vec{\mathbf{F}}$ is the corresponding flux vector that includes both convective and viscous fluxes as well as the effect of a moving control volume via mesh velocities. The mesh velocities are incorporated since the equations are solved in a laboratory inertial frame of reference. The semi-discrete form of this equation is obtained by discretizing only the spatial part and can be expressed as

$$D_t \mathbf{U} + R(\mathbf{w}) = 0, \quad \mathbf{U} = \int_{\Omega} \mathbf{w} dV, \quad (1)$$

where \mathbf{U} is assumed to vary in time because of changes in the actual flow solution and due to control volume variations that result from mesh deformations.

One of the various ways to solve Equation 1 is by casting it as a steady-state problem in pseudo-time. This can be accomplished by using the time derivative term as a solution-dependent source term in a pseudo-time iteration. With the addition of a fictitious pseudo-time derivative term, the advancement of the solution to the next physical time step is achieved by marching these equations forward in t^* until a steady-state (in pseudo-time) has been reached. Namely, the following problem is solved

$$\frac{\partial \mathbf{U}^n}{\partial t^*} + D_t \mathbf{U}^n + R(\mathbf{w}^n) = 0, \quad (2)$$

where n is the index of the physical time step.

The next few sections discuss the different ways that can be used to discretize the time derivative term, D_t .

B. Backward Difference Formula(BDF)

The second-order A-stable BDF⁴ scheme treats the time derivative term in the following way

$$D_t \mathbf{U}^n = \frac{3\mathbf{U}^n - 4\mathbf{U}^{n-1} + \mathbf{U}^{n-2}}{2\Delta t}, \quad (3)$$

where Δt is the physical time step and n is index of the time instance. Note that the current solution that is being computed at time step n depends only on the solution at the two previous time instances, $n - 1$, and $n - 2$. This is a general purpose scheme and can be applied to generic unsteady problems that need not be periodic. In our work, the advancement of the solution at each physical time step is achieved using a number of inner multigrid iterations in t^* . Because of the co-existence of physical and pseudo time, this solution approach has often been called the dual-time stepping BDF scheme. Since the scheme is A-stable, the physical time step, Δt , can be chosen to be arbitrarily large. In practice, however, Δt is chosen such that the relevant time scales of interest are captured accurately. Typical turbomachinery problems require 50-100 time steps per blade passing for sufficient accuracy. Combined with 25-50 inner multigrid iterations for every time step (to reduce the magnitude of the residual sufficiently) and 4-6 revolutions to reach the periodic state for a high RPM machine, this scheme can be very expensive. For highly-stretched meshes typical of high-Reynolds number viscous calculations, however, this implicit scheme can be significantly less expensive than the explicit alternative. Note that the system in Equation 1 can be solved with a variety of different schemes. There is strong evidence that using a Diagonally-Dominant Alternating Direction Implicit driver in combination with multigrid for the inner iterations can result in significantly faster convergence than is achieved with the combination of multigrid and a modified Runge-Kutta scheme that we have used in this work.

C. Time Spectral Method for Periodic Problems^{5,21}

The Time Spectral method was developed specifically for time-periodic problems. It uses a Fourier representation in time for the unsteady variation of the solution at each point in the computational domain. In the case of a turbomachine, the problem is naturally periodic with a periodic sector that encompasses the entire wheel. Depending on the actual blade counts a fraction of the entire wheel may also be used as the periodic section. In these situations, periodic boundary conditions can be applied in time. In this section we briefly present the fundamental idea behind the Time Spectral method. If the periodic time interval T is divided into time levels (we introduce the notation *time levels* to indicate the sub-intervals of the periodic interval) at which the solution is desired, a Fourier series can be constructed for every flow variable in every computational cell in the mesh for the entire time period. The discrete Fourier transform of such signals over a time period T is given by

$$\hat{U}_k = \frac{1}{N} \sum_{n=0}^{N-1} U^{*n} e^{-i(k\frac{2\pi}{T})t_n},$$

where T has been divided into N equal time intervals, n is the index of the time level, and k is the wave number. \mathbf{U}^* is the N -vector that describes the time variation of a single flow variable at a given location in the computational mesh throughout the time period, i.e. $\mathbf{U}^* = [U_{t_0}, U_{t_1}, \dots, U_{t_{N-1}}]^T$ and $\hat{\mathbf{U}}$ is the vector of Fourier coefficients, $\hat{\mathbf{U}} = [\hat{U}_0, \hat{U}_1, \hat{U}_2, \dots, \hat{U}_K, \hat{U}_{-K}, \dots, \hat{U}_{-1}]^T$. K is the highest wave number that N time instances can accommodate and is equal to $(N - 1)/2$ for odd values of N . The Fourier transform can also be written as a matrix-vector product, $E\mathbf{U}^*$, where E is the Fourier matrix whose elements are

$$E_{k,n} = \frac{1}{N} e^{-i(k-1)\frac{2\pi}{T}t_n}. \quad (4)$$

The inverse Fourier transform relating the \mathbf{U}^* and $\hat{\mathbf{U}}$ is simply the inverse operation using E^{-1} which also has an analytic expression,

$$E_{n,k}^{-1} = e^{i(k-1)\frac{2\pi}{T}t_n}. \quad (5)$$

The time derivative operator D_t applied to \mathbf{U}^* would amount to

$$D_t \mathbf{U}^* = D_t(E^{-1}E\mathbf{U}^*) = D_t(E^{-1}\hat{\mathbf{U}}) = \frac{\partial E^{-1}}{\partial t} \hat{\mathbf{U}} = \frac{\partial E^{-1}}{\partial t} E\mathbf{U}^*,$$

and hence

$$D_t = \frac{\partial E^{-1}}{\partial t} E. \quad (6)$$

A simpler form of this combined operator has been derived by Gopinath and Jameson^{21,22} and rewrites D_t as a matrix operator whose elements (for odd N) are

$$d_{j,n} = \begin{cases} \frac{2\pi}{T} \frac{1}{2} (-1)^{j-n} \operatorname{cosec}\left(\frac{\pi(j-n)}{N}\right) & : n \neq j \\ 0 & : n = j. \end{cases}$$

In principle this algorithm can be applied to the true turbomachinery geometry to be solved, namely the entire periodic section, whether it is the full wheel or a portion of it. However this would be a very expensive proposition because the time derivative term couples all the time instances. This requires the simultaneous storage of the solution at all N time instances at every spatial grid point, unlike the second-order BDF scheme that only requires that the solution at the two previous time instances be stored. Hence this algorithm is normally used in combination with a scaled geometry, so that a periodic fraction of the annulus is solved and the storage requirements are minimized. Even after this reduction in spatial size, if the number of time instances needed to resolve the unsteady phenomena in question is larger than $O(10)$, then the savings compared to solving the rescaled problem using the BDF scheme become marginal.

D. Harmonic Balance method

1. Frequencies and Time Derivative Matrix

It is common knowledge in the turbomachinery community that the dominant frequencies seen by a blade row are those created by the passing of the neighboring blades. For instance, in an isolated single stage setup with the stator row following the rotor row, the rotor row perceives the blade passing frequency of the stator row and its higher harmonics and the stator row correspondingly resolves the rotor's blade passing frequency and its higher harmonics. Hence each blade row resolves only a single fundamental and its harmonics. In contrast, a multi-stage case is more complicated. In such cases, each blade row is sandwiched between neighboring blade rows and sees blade passing frequencies from all its neighbors. If the blade counts of the neighbors are different, which is the case in most practical turbomachines, these blade passing frequencies could be different. The sandwiched blade row then resolves various combinations (addition and subtraction of multiples of the various frequencies) of the frequencies. This leads to a situation where there is not one fundamental frequency but several of them in addition to their higher harmonics. A set of frequencies to be resolved in each blade row is specified as an input to the Harmonic Balance algorithm which can then be used to predict the unsteady flow through a turbomachine at only a fraction of the cost of the BDF scheme.

It is well known from the classic paper by Shannon²³ that a minimum of $2K + 1$ equally spaced grid points are required to resolve K harmonics of the fundamental frequency. Along the same lines, we choose to resolve a time span that is equal to the time period of the lowest frequency resolved in each blade row and, if K frequencies are resolved in a blade row, the time span is divided into $N = 2K + 1$ time levels. As mentioned before, each blade row could resolve different frequencies (depending on the blade counts of its neighbors) and hence use different time spans and correspondingly different time instances. This is the fundamental difference between the Harmonic Balance and Time Spectral methods: in the Time Spectral method all blade rows solve for the same time instances and over the same time span (equal to the time period of revolution) whereas in the Harmonic Balance method both the time instances / levels and the time span can be different.

The governing equations are solved in a very similar way to that used for the Time Spectral method, where the time derivative term is used as a source term and the equations are marched in pseudo-time to a periodic steady state. The structure of D_t is explained as follows. Recall the expression for the time derivative matrix in Equation 6, derived for the Time Spectral method. The Harmonic Balance method uses the same form but a different definition of the Fourier matrices E and E^{-1} .

As mentioned before, for a periodic problem with time period T , the Time Spectral method resolves the fundamental frequency, $w_1 = \frac{2\pi}{T}$ and its higher harmonics. In such a case, the matrix E can be written as (recall Equation 4)

$$E_{k,n} = \frac{1}{N} e^{-i(k-1)w_1 t_n}.$$

In the Harmonic Balance case, especially in a multistage situation, the frequencies are not integer multiples of each other and hence the matrix E takes the form

$$E_{k,n} = \frac{1}{N} e^{-i w_{k-1} t_n},$$

and E^{-1} is computed from E . The expression for the time derivative term, D_t , then becomes

$$D_t = \frac{\partial E^{-1}}{\partial t} E.$$

It must be noted that it is easier to first construct E^{-1} analytically (and hence have an analytic expression for the derivative) and then compute E as its inverse. The various frequencies to be resolved, w_k , are given by

$$\mathbf{w} = [w_0, w_1, w_2, \dots, w_K, w_{-K}, \dots, w_{-1}]^T,$$

where w_0 is always the zeroth harmonic, $w_0 = 0$ and the frequencies with a negative wave number are $w_{-k} = -w_k$. Thus there are only K independent frequencies and hence \mathbf{U}^* is always real. For real U^* , one could halve the number of variables stored and avoid the complex arithmetic. We shall use this convention just for clarity. It is evident that once the frequencies are chosen, all other parameters including the number of time instances, N , the time span over which solution is sought, etc., fall in place. The frequencies are specified in the following way. The k^{th} frequency resolved in blade row j is given by,

$$w_k^{rowj} = \sum_{i=1}^{nRows} n_{k,i} B_i (\Omega_j - \Omega_i). \quad (7)$$

Here B_i is the blade count of the i^{th} blade row and Ω_i , the rotation rate of the i^{th} blade row. $\Omega = 0$ for stators. $n_{k,i}$ takes on integer values that are specified as an input to the solution procedure by the user. Hence K sets of combinations are specified for K frequencies. A few points can be noted from this equation. Only neighbors contribute to the frequencies considered by a blade row. A neighbor which is stationary with respect to a blade row does not contribute to its temporal frequency.

2. Periodic Boundary Conditions

In the previous section we have shown how we contained the problem size by reducing the time span over which the solution is sought. In this section, we present the way in which we use a computational grid that spans only one blade passage per blade row compared with the periodic sector that was required by the Time Spectral method.

Since, in principle, we do not have a periodic sector anymore, the azimuthal boundaries of a blade passage no longer satisfy periodic boundary conditions. We will modify the boundary conditions in a manner similar to the phase-lagged condition,^{11,12} which states that

$$\mathbf{U}(\theta, t) = \mathbf{U}(\theta + \theta_G, t'), \quad (8)$$

where $t' = t - \delta t$ and δt is related to the inter-blade phase angle. In other words, the flow field at an azimuthal distance shifted by the blade gap (θ_G), can be generated from the computed flow field at a different time.

Expanding the flow variables in the form of a Fourier series both in time and the azimuthal direction, one can write,

$$\mathbf{U}^*(x, r, \theta, t) = \tilde{\mathbf{U}}(x, r) \sum_{n=0}^{N-1} \sum_{m=0}^{M-1} e^{-i(\mathbf{w}t_n + \mathbf{N}\theta_m)}, \quad (9)$$

where \mathbf{N} is the vector of nodal diameters N_k , an equivalent of the w_k in the azimuthal direction. These are given in terms of the combinations specified for w_k and are,

$$N_k = \sum_{i=1}^{nRows} n_{k,i} B_i.$$

The nodal diameters are another way of representing the δt in the phase-lagged condition (Equation 8). Equation 9 can be rewritten in terms of the Fourier coefficients $\hat{\mathbf{U}}$ as,

$$\mathbf{U}^*(x, r, \theta, t) = \hat{\mathbf{U}}(x, r, \theta) \sum_{n=0}^{N-1} e^{-i\mathbf{w}t_n}. \quad (10)$$

Comparing equations 9 and 10,

$$\hat{\mathbf{U}}(x, r, \theta) = \tilde{\mathbf{U}}(x, r) \sum_{m=0}^{M-1} e^{-i\mathbf{N}\theta_m},$$

and hence,

$$\hat{U}_k(x, r, \theta + \theta_G) = \hat{U}_k(x, r, \theta) e^{-iN_k\theta_G}.$$

This modified periodic boundary condition is applied to the upper and lower azimuthal boundaries of a single blade passage and relates the temporal Fourier coefficients at two azimuthal locations shifted by the blade gap.

3. Sliding Meshes and Multistage Coupling

In this section, we discuss how information is passed from one blade row to its upstream or downstream neighbor through the use of sliding mesh interfaces. In the case of the Time Spectral and BDF schemes, the unsteady solution at the exact same time instances was computed in each blade row. If the whole wheel was simulated, there was always a donor cell in the adjoining blade row. When only a periodic fraction of the annulus was solved for and due to relative motion of the blade rows, it is possible that a physical donor does not exist on the neighbor's side and the donor's information was generated using periodic boundary conditions. These interpolation procedures, although complicated by the parallel decomposition of the solver, were relatively straightforward.

The situation in the Harmonic Balance method is more complicated. First of all, just like in the Time Spectral case, the flow field in the neighboring blade row must often be generated using the modified periodic boundary conditions discussed in the previous subsection. Secondly, as mentioned earlier, different frequencies are resolved in adjoining blade rows and hence solutions at different instances in time are sought in these rows, i.e. the n^{th} time instance in row_i and row_{i+1} need not correspond to the same physical time. Consequently the donor's information has to be generated at both the spatial location and physical time corresponding to the receiver's cell.

In the original implementation of the Harmonic Balance method^{16,19} this coupling was done in the frequency domain. On an interface, the flow variables \mathbf{U}^* on the donor blade row side are Fourier transformed in time to get $\hat{\mathbf{U}}$ (Equation 2) at each azimuthal location. Since azimuthal grid lines need not match across the interface, another Fourier transform was performed in the θ direction to get $\tilde{\mathbf{U}}$. Assuming radially matched grid lines, these coefficients were transferred to the receiving blade row after applying non-reflecting boundary conditions¹⁸ to eliminate spurious reflections due to frequencies that were not included in the specified frequency set. Using the basis set of w_k and N_k on the receiver's blade row side, \mathbf{U}^* was computed from the Fourier coefficients.

In the current version of the algorithm, we choose to couple adjoining blade rows purely in the time domain, making it a pseudo-spectral method. This choice was made to avoid the use of complex arithmetic and to re-use the interpolation machinery already coded in the SUMB solver. The flow field on the donor side needs to be generated for all the times corresponding to the receiver side. This is done using trigonometric interpolation in time. The simplest way to do this is to work with the Fourier coefficients,

$$\mathbf{U}^*(t^{receiver}) = \bar{E}^{-1} E \mathbf{U}^*(t^{donor}),$$

where

$$E_{k,n} = \frac{1}{N} e^{-iw_{k-1}t_n^{donor}},$$

but,

$$\bar{E}_{k,n}^{-1} = e^{iw_{k-1}t_n^{receiver}}.$$

Note that at these interpolated times, the azimuthal location of the physical donor need not match with the receiver and hence has to be generated using the modified periodic boundary conditions. This situation has been discussed earlier in the paper.

During interpolation and exchange of basis sets between blade rows, higher frequencies are generated. On a grid with $N = 2K + 1$ time points, only K frequencies can be captured. Higher frequencies alias onto the lower frequencies and corrupt the information present in the basis set. Once corrupted, there is no way to get rid of these spurious frequencies. This aliasing instability worsens with time and can render the entire scheme unstable. This form of instability has been studied in great detail in the field of spectral methods and is typical of pseudo-spectral methods. One of the conventional ways of dealiasing is by using Orszag's "Two-Thirds Rule".²⁴ The essence of the method is to capture these higher frequencies using a longer stencil and then "filter" them out. i.e., in order to capture K frequencies, instead of using $2K + 1$ points, we use $3K + 1$ points. In this way the higher frequencies will be captured in the last K wave numbers, without corrupting the smaller wave numbers. The coefficients of the last K Fourier coefficients are then set to zero (zero padding) before transforming back to physical space.

Solving for $N = 3K + 1$ time instances in all blade rows and at every spatial grid point in order to avoid the aliasing problem at the interface, might be unnecessary. It was also shown by van der Weide, Gopinath and Jameson⁵ that using $N > 2K + 1$ introduces additional zero eigenvalues for the time derivative term. These could be responsible for odd-even decoupling between the time instances and cause instability problems, especially in high RPM turbomachinery cases.

Instead, we use more than $2K + 1$ time instances only at the interface for interpolation purposes. Time interpolated data from the donor side is requested not at $2K + 1$ time instances (corresponding to the receiver side), but at twice that many instances: one extra time instance between every two time instances for which the solution is calculated. These half-way intermediate points are chosen just for ease such that the original time instances can be used and equally spaced points can be used for the Fourier transform while keeping the overall time span the same. According to the two-thirds rule, K more time instances would suffice to capture the higher frequencies. The spurious higher frequencies can now be captured on these $2(2K + 1)$ time instances without corrupting the lower wave numbers. The data on the receiver side now has to be filtered such that only the $2K + 1$ frequencies we are interested in are used for the rest of the computation. Zero padding is done by multiplying \mathbf{U}^* with the matrix E which consists of only the lower frequencies, then transforming back to physical space to get the filtered data. Hence,

$$U_{filtered}^* = E^+ E U_{unfiltered}^* \tag{11}$$

where U^* is of length $2(2K + 1)$. Thus E is not square anymore: its size is $(2K + 1) \times 2(2K + 1)$, i.e., it is evaluated at $2(2K + 1)$ time instances but includes only $2K + 1$ frequencies w_k . Hence E^+ , the pseudo-inverse of E , replaces E^{-1} in Equation 11. Note that $E^+ E$ on this extended stencil is not the identity matrix, I but is equivalent to the zero padding operation.

III. RESULTS

In this section, we present results for two test cases computed using the Harmonic Balance method that has been discussed in this paper. The first one, a single-stage case, is the three-dimensional NASA Stage 35 compressor rig, while the second one, Configuration D, is a two-dimensional model of a multi-stage compressor geometry.

The flow solver used in this work is Sumb (Stanford University multi-block), a compressible multi-block URANS solver developed at Stanford University during the Department of Energy's ASC (Advanced Simulation and Computing)²⁵ Program. Sumb uses a cell-centered finite volume formulation and a variety of central-difference and upwind schemes. In this work, the inviscid fluxes are computed using a central difference scheme augmented with a standard scalar formulation for the artificial dissipation terms.²⁶ The viscous fluxes are computed using central differencing. Convergence is accelerated using a standard geometric

multigrid algorithm in combination with an explicit multi-stage Runge-Kutta scheme. Several different turbulence models are available in Sumb. For our viscous test case, the NASA Stage 35 compressor rig, we use the one-equation Spalart-Allmaras²⁷ turbulence model. The turbulence equations are solved in a segregated manner from the mean flow using a Diagonally-Dominant Alternating Direction Implicit (DD-ADI) discretization²⁸ as the basic iterative method.

A. NASA Stage 35 Compressor²⁹

This low aspect ratio transonic compressor has 36 rotor blades rotating at 17,119 RPM (at its operating point) and 46 stator blades. The geometry that is used for the Harmonic Balance computations consists of a single blade passage per blade row and is depicted in Figure 1. The computational mesh has 8 blocks and a total of 1,842,176 cells. A turbulent viscous grid is used and the spacing normal to the viscous boundaries is such that the maximum y^+ value is of the order of $\mathcal{O}(1)$. Uniform inflow boundary conditions are applied: the flow is assumed to be axial at the inlet and a total pressure of 101.3kPa and a total temperature of 288K are specified. An outlet static pressure of 101.3kPa is also prescribed.

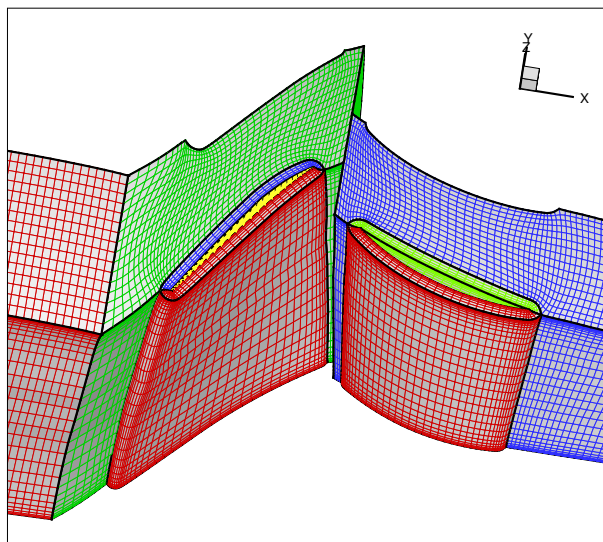


Figure 1. Multiblock structured mesh of the NASA Stage 35 Compressor used for the HB computation (Every alternate grid line shown for clarity)

The NASA Stage35 test case is a single-stage case with just one rotor blade row followed by a single stator blade row. Hence, the frequencies resolved in the rotor are the blade passing frequency of the stator and its higher harmonics while those resolved in the stator are the blade passing frequency of the rotor and its higher harmonics. Thus if $K = k$ frequencies are resolved in this computation in both the rotor and stator blade passages, the values taken by $n_{k,i}$ in Equation 7 can be seen in Table 1. For this test case, we have performed computations for values of $K = 1, 2, 3, 4$ and 5 frequencies to assess the convergence of the Harmonic Balance procedure as the number of retained frequencies is increased.

n Rotor	n Stator
1	1
2	2
3	3
·	·
·	·
k	k

Table 1. Frequency Combinations for the Single Excitation Frequency case

Figures 3(a) and 3(b) depict the instantaneous pressure and entropy distributions on a surface at constant radius (from the axis of the rig) halfway between the hub and the case using 4 frequencies. The multiple passages shown in this and subsequent Figures have been post-processed from a computation using only one blade passage per blade row to facilitate the interpretation of the output. The entropy distribution clearly shows the wakes from the rotor impinging on the stator, an effect that is completely lost in the mixing plane solution shown in Figure 2(b). A strong shock is seen in the rotor blade row that leads to flow separation due to shock wave-boundary layer interaction. This effect is clearly seen in the large increase in the value of the entropy in the suction side of the blade. When the corresponding wake impinges on the suction side of the stator blade, a complex unsteady flow field results. Near the casing a large separation bubble is observed, much larger than the mixing plane solution predicts. Figures 4(a) and 4(b) show this three-dimensional effect. They depict entropy contours at two other surface locations at constant radii that surround the location of the original Figure. The wakes themselves rotate as they move through the stator passages, an effect caused by the velocity difference between the suction and pressure sides of the blades.

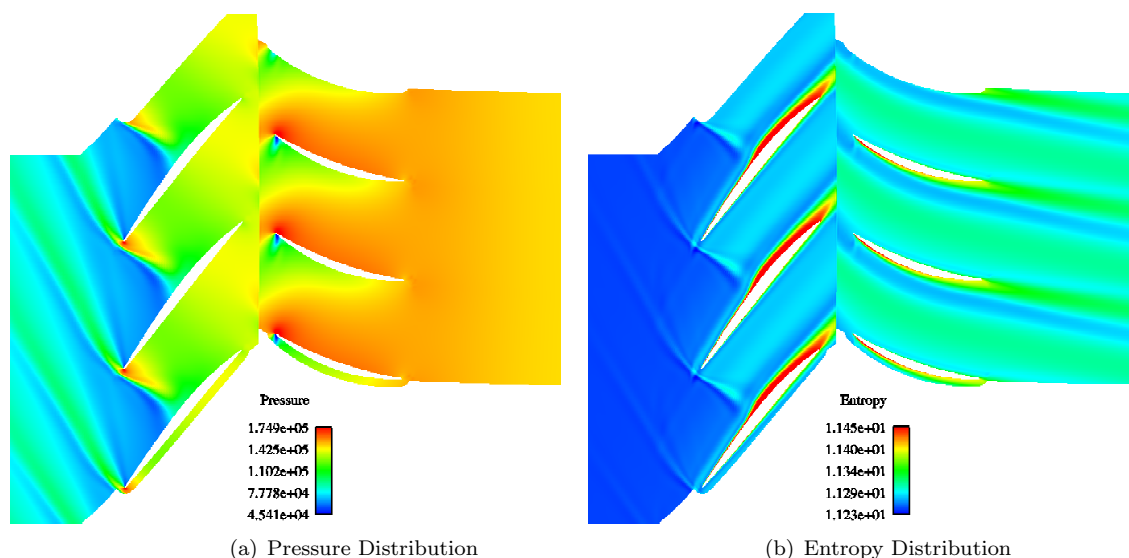


Figure 2. NASA Stage35 compressor: pressure and entropy distribution on a surface at constant radius half way between the hub and the casing($R=8.5$) using a Mixing Plane computation

Figures 5(a) and 5(b) show the variation of the magnitude of the force and the torque on the rotor blade computed using increasing values of K . The force and torque are plotted as a function of time over a time span equal to the time period of the lowest frequency resolved (namely, the blade passing of stator). These Figures show that 3 harmonics are able to predict the force on the rotor blade quite well since there is hardly a difference with the computations that include 4 and 5 harmonics. Similarly Figures 6(a) and 6(b) show the force and torque variations on the stator blade. The exact resolution of the forces and moments on the stator requires 4 frequencies: a higher frequency content than for the rotor row. This is because the downstream stator blade row resolves the blade passing of the rotor and this predominantly consists of the wakes that run downstream from the rotor. This wake further propagates through the stator passage stretching and rotating, complicating the flow field.

The force variation plots also show the steady force predicted by the mixing plane technique. The force and torque on the rotor blade predicted by the mixing plane method are fairly close to the Harmonic Balance solution at $t=0$. This is also evidenced in the instantaneous pressure and entropy distribution. Except very close to the interface between the two blade rows, the solution in the rotor blade row at $t=0$ is well captured by using just the mixing plane procedure (Figures 2(b) and 3(b)). However, this is not the case with the stator blade row. The unsteadiness in the stator row is directly influenced by the upstream rotor and hence a

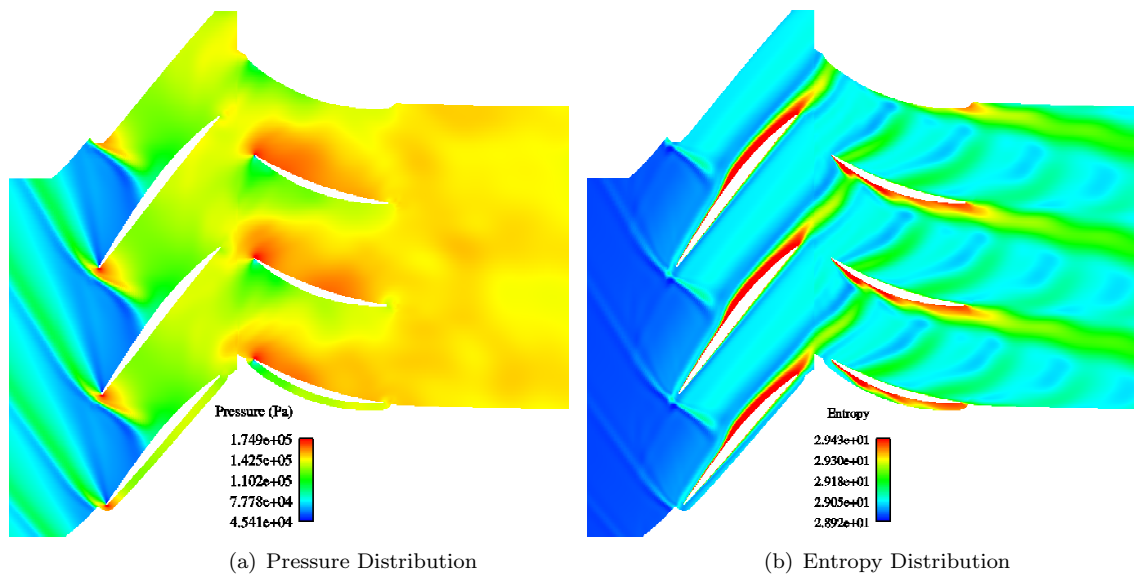


Figure 3. NASA Stage35 compressor instantaneous pressure and entropy distribution on a surface at constant radius half way between the hub and the casing($R=8.5$) using the Harmonic Balance Technique($K=4$)

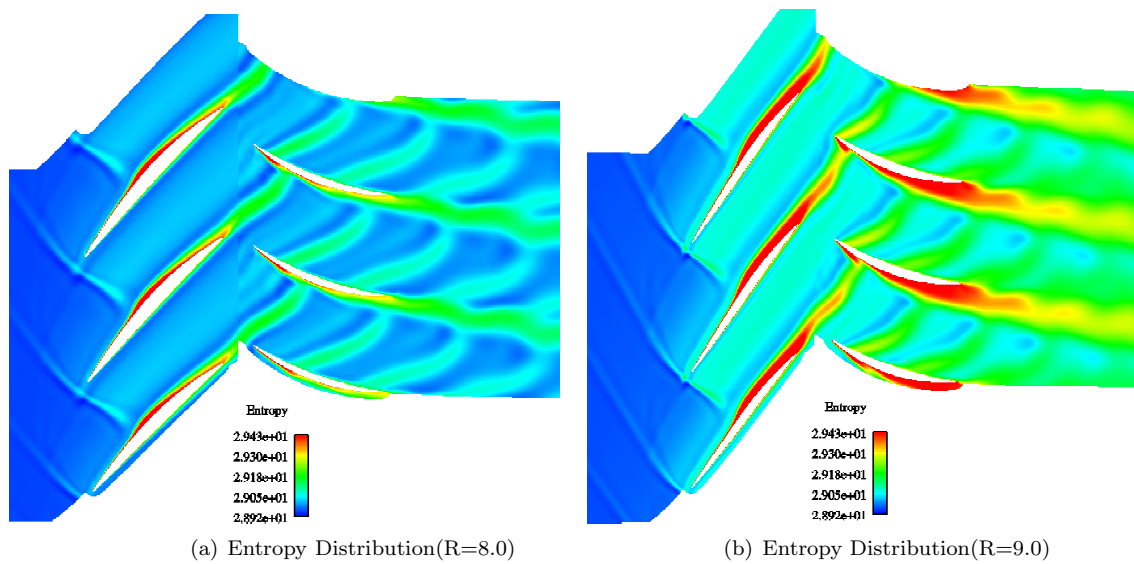


Figure 4. NASA Stage35 compressor instantaneous entropy distribution at two different surface locations($R=8.0$ and $R=9.0$) using the Harmonic Balance Technique($K=4$)

mixing plane solution is insufficient to capture its features. Notice that in all cases the mixing plane solution is not necessarily representative of the average of the unsteady solution as it does not contain any of the flow features that lead to the unsteady variation. The errors in the force and torque values are anywhere between 2-5% with the larger errors found in the stator blade. This level of error may or may not be significant depending on the objective of the calculations being performed. Note also that although 3 and 4 harmonics are required in the rotor and stator to resolve the values of forces and moments accurately, even the use of a single harmonic would bring these errors to well within a half a percentage point. This brief discussion simply goes to illustrating the point that the Harmonic Balance method being proposed is indeed a reduced-order model where the accuracy of the computation can be traded against its cost. However, for computations that are strongly dominated by a small set of frequencies, relatively crude reduced-order models may lead to highly-accurate simulations.

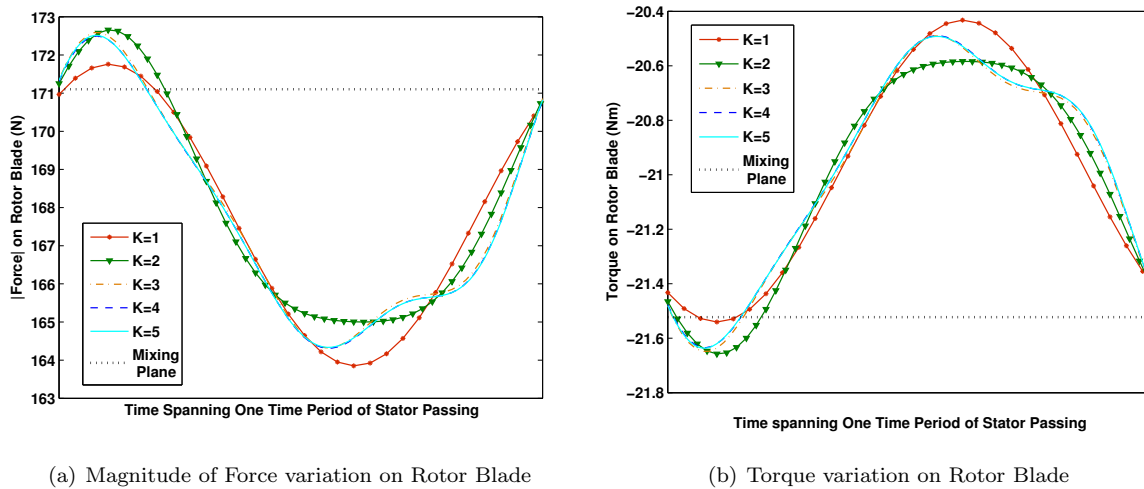


Figure 5. NASA Stage35 compressor force and torque variation on rotor using Harmonic Balance method(various number of frequencies). Plotted as a function of time spanning one time period of stator passing.

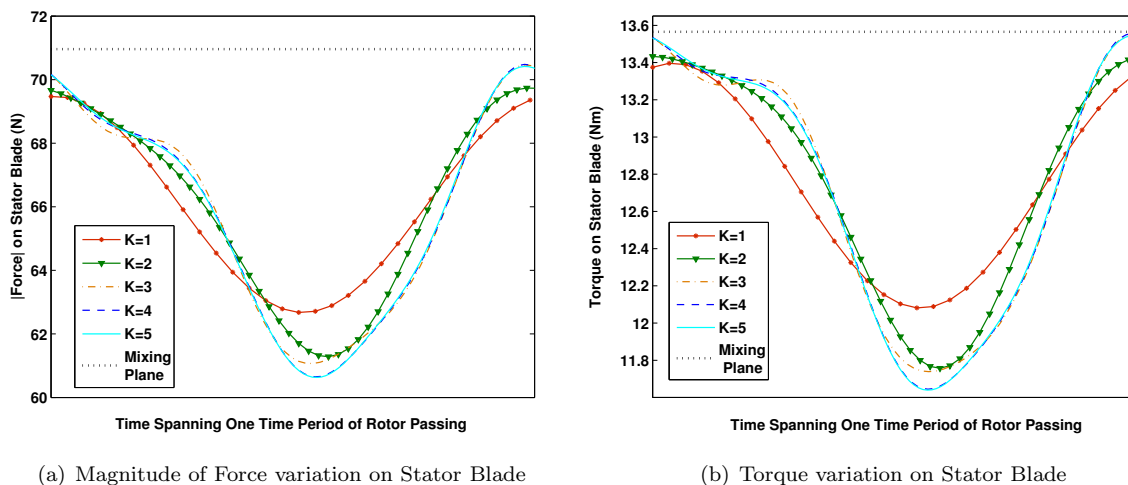


Figure 6. NASA Stage35 compressor force and torque variation on stator using Harmonic Balance method(various number of frequencies). Plotted as a function of time spanning one time period of rotor passing.

Computations on a scaled 1-1 configuration with 36 rotor blades and 36 stator blades were performed using the Time Spectral method and were presented in an earlier paper.⁵ A time convergence/resolution

study had shown that the rotor required 7 time instances (the equivalent of 3 frequencies) to produce accurate results. This is consistent with our observations in this work. For the stator, our previous work using the Time Spectral method required at least 11 time instances (5 frequencies) for time convergence. Although very much consistent with our observations here, the Time Spectral method appeared to require slightly more time instances. It should be noted, however, that in that work a scaled geometry (and hence a different problem) was being solved for.

The convergence history of the residuals for the Harmonic Balance calculations are shown in Figure 7. The mixing plane method is used to provide an initial solution for the Harmonic Balance method that uses $K = 1$ frequency. For the higher frequency cases, the ideal initial condition would be the interpolated solution from the lower frequency content case. This option hasn't been implemented yet and hence the solution at the first time instance is rotated to obtain the initial guess for the higher frequencies.

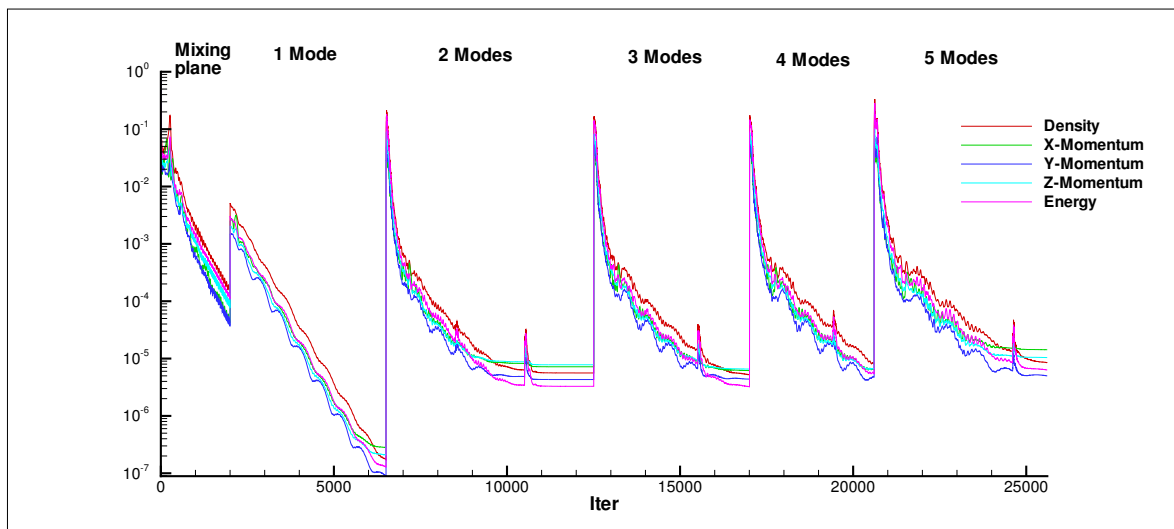


Figure 7. NASA Stage35 Test Case: Convergence History using various number of frequencies.

The Harmonic Balance computations were performed on a 64 bit 3.6GHz Pentium Linux cluster with an Infini-band interconnect. The $K=1$ computation required a total of about 350 CPU hours to converge 5 orders of magnitude in all residuals. The CPU time of the other computations (with higher values of K) scaled linearly with increasing number of frequencies. A comparable BDF computation could be performed on half the annulus (18 rotors and 23 stators) and hence is about 20 times the size of the problem currently solved in the Harmonic Balance method. At least 50 physical time steps per blade passing and about 50 multigrid iterations per time step would be required in combination with 3-4 periodic revolutions for a periodic state to be arrived at. On the same Linux cluster, this would cost an estimated 150,000 CPU hours. This clearly suggests a two-order of magnitude savings in CPU time for the Harmonic Balance method over a time-accurate BDF scheme.

B. Configuration D: two-dimensional multistage compressor

This model two-dimensional compressor geometry has 5 blade rows. The flow parameters for this geometry are specified in Ekici and Hall.¹⁶ For our present work, we will use a geometry consisting of the middle three blade rows, a stator followed by a rotor and another stator. Their pitches are in the ratio 1.0:0.8:0.64. The grid consists of 3 blocks and a total of 18,432 cells (see Figure 8). Euler computations were performed on this grid and hence only acoustic and vortical interactions between the blade rows were observed. Note that all results presented for this case are in non-dimensional units; the lengths are non-dimensionalized by the chord of the rotor blade, velocities by the relative inflow velocity to the rotor blade row and the pressures by the dynamic pressure at the inflow of the rotor blade row.

As before, a mixing plane computation is used as the initial condition for the Harmonic Balance method. The two stators do not move relative to each other and have only one neighbor, the rotor, and hence resolve only the blade passing of the rotor and its higher harmonics. On the other hand, the rotor has two

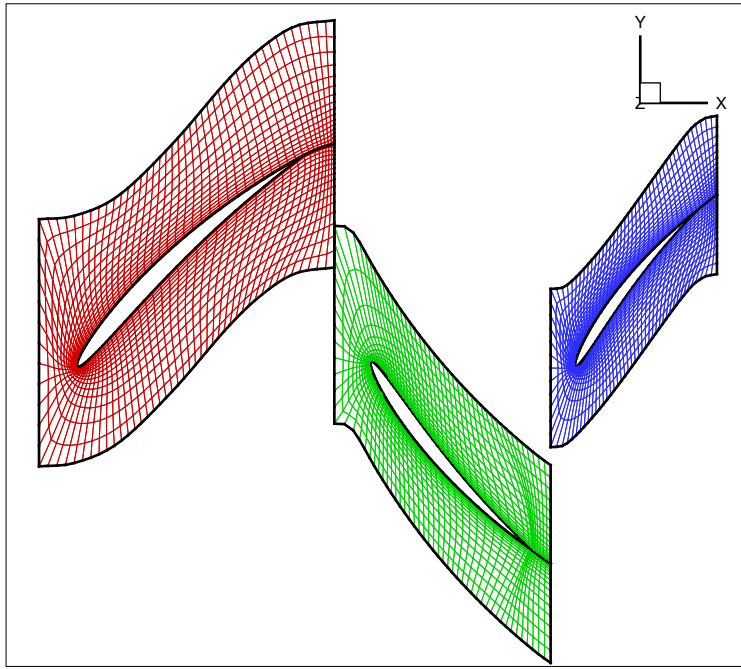


Figure 8. Multiblock structured mesh of Configuration D (middle three blade rows) used for the HB computation (Every alternate grid line shown for clarity)

neighbors with different pitches, and hence resolves frequencies that are combinations of the two stator blade passings. A typical frequency combination table is shown in Table 2. Figures 9(a), 9(b) and 9(c) show the instantaneous pressure distribution computed using $K=2$ ($BPS1$ (blade passing of Stator1) and $BPS2$ (blade passing of Stator2)), $K=4$ ($BPS1$, $BPS2$, $BPS1+BPS2$ and $BPS1-BPS2$) and $K=7$ ($BPS1$, $BPS2$, $BPS1+BPS2$, $BPS1-BPS2$, $2*BPS1$, $2*BPS1-BPS2$ and $2*BPS1+BPS2$) respectively. Again, the solution on adjacent passages within the same blade row have been post-processed using the single passage solution for easier understanding of the output. Observe that using only the frequencies corresponding to the blade passing ($K=4$), the macroscopic features are already captured. Increasing the number of frequencies obviously improves the quality of the solution. The solution across the blade row interface is slightly discontinuous. This is to be expected since adjoining blade rows use different basis sets and resolve only a subset of all the frequencies that the blade rows should resolve.

Information about all the frequencies that need to be resolved can be obtained from a time-accurate calculation using the BDF scheme on the true geometry (in this case a fraction of the wheel with 16 Stator1, 20 Rotor and 25 Stator2 blade passages.) The pressure distribution from such a solution is shown in Figure 9(d) at the same instance as in Figures 9(a) or 9(b) or 9(c). Again, comparing the solution from the Harmonic Balance method, the macroscopic features are well captured while obtaining a solution at fraction of the cost.

This BDF computation required 50 time steps per blade passage of Stator2 and 25 inner multigrid iterations per time step. Three revolutions were necessary to reach periodic state as shown in Figure 10. This figure shows the convergence of the magnitude of the force to a periodic state (every 25th physical time step is plotted and hence this Figure is not an accurate representation of the resolved frequencies). The forces on the two stators suggest the presence of a dominant frequency that is not as obvious on the rotor. The force on the rotor is, of course, periodic with the time period of the annulus. The frequency content of this force variation over the time period is shown in Figure 12. As examined in Figure 10 the two stators resolve only one fundamental frequency, the rotor blade passing, whereas the force on the rotor consists of a multitude of frequencies, not necessarily multiples of each other. A few dominant frequencies are pointed out in the figure as combinations of the two stators blade passings. Note that the most dominant ones are $BPS1$ and $BPS2$ which are the ones resolved in the $K = 2$ computation.

Figures 11(a) and 11(b) plot the force variation on the rotor blade as computed by the BDF scheme and by the Harmonic Balance technique using $K = 2, 4$ and 7 frequencies. Only a fraction of the time period of

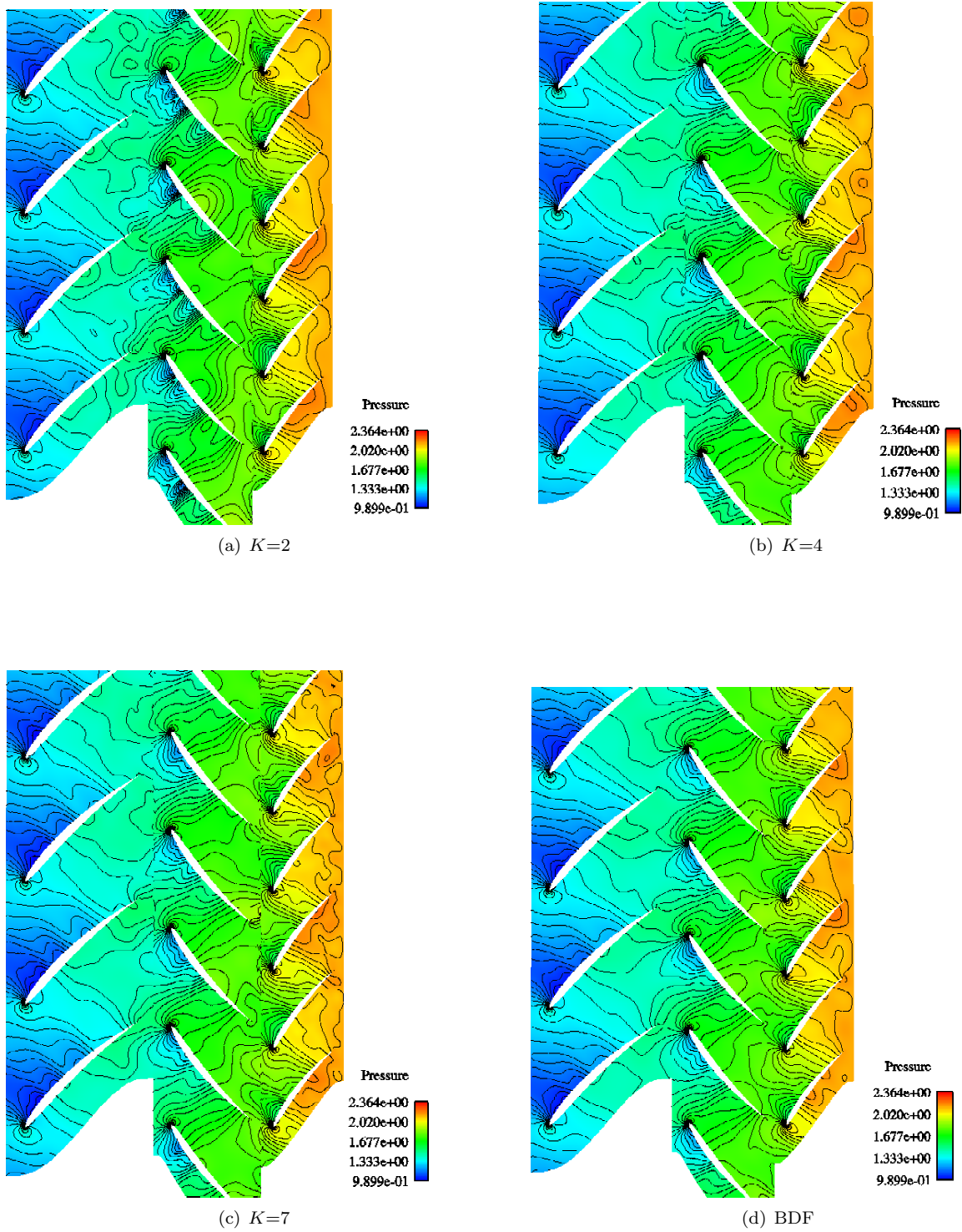


Figure 9. Configuration D: Instantaneous pressure distribution computed using Harmonic Balance method (various number of frequencies) and the time-accurate BDF scheme.

Case	n Stator1	n Rotor	n Stator2
K=2	1	1	0
	0	2	1
K=4	1	1	0
	0	2	1
	1	3	1
	1	4	-1
K=7	1	1	0
	0	2	1
	1	3	1
	1	4	-1
	2	5	0
	2	6	-1
	2	7	1

Table 2. Frequency Combinations for the Multiple Excitation Frequency case

the whole annulus has been plotted for clarity (hence, the forces are not periodic with the time span plotted). It is observed that all the Harmonic Balance calculations predict the forces within 10% of the BDF solution, regardless of the frequency content retained. Time convergence is obtained when the number of frequencies in the specified set is increased ($K = 7$ is able to capture most of the deviations off the mean quite closely to the BDF solution, see Figure 11(b)). For the case of $K = 7$, the maximum errors are of the order of 2-3% only.

On the same Pentium Linux cluster used to run the Stage 35 test case, the BDF computation for this Configuration D test case required about 290 CPU hours. While the Harmonic Balance technique using $K = 7$ frequencies converged 7 orders of magnitude in 33 CPU hours. This clearly indicates an order of magnitude savings in CPU time while maintaining reasonable accuracy. It is almost futile to perform a time accurate calculation like this one to predict the dominant frequencies for a viscous three-dimensional practical multi-stage turbomachine. We have performed this BDF computation on a relatively small problem only to illustrate the typical frequencies present in turbomachinery problems. We have shown that the dominant frequencies are combinations of the blade passing of the neighboring row and hence justify the choice of frequencies in the Harmonic Balance method.

IV. CONCLUSIONS AND FUTURE WORK

In this paper, we have extended the Harmonic Balance method so that three-dimensional unsteady Euler and RANS multi-stage turbomachinery calculations can be performed using a purely time-domain method. This is done while maintaining accuracy and keeping computational costs low. Further reductions in cost can be made available by small sacrifices in the required accuracy of the computation. Costs are kept low by using a Fourier representation in time such that a periodic state is directly reached without resolving transients. The spatial size of the problem is drastically reduced by using a single passage per blade row for the computational grid. Accuracy is maintained by choosing to resolve only the dominant frequencies of all blade rows (essentially the blade passing frequencies of its neighbors). A set of specified frequencies are resolved in each blade row and this set can be customized by the analyst / designer based on a trade-off between accuracy and computational cost. Interaction between blade rows is done via sliding mesh interfaces where we perform both spatial and spectral time interpolations. Nonlinear effects in combination with spectral interpolation give rise to aliasing errors which have been treated properly to ensure the stability of the computation at these interfaces. The coupling across the sliding mesh interfaces is done purely in the time domain such that an already existing code, Sumb, can be readily used.

For a simple Euler calculation on a two-dimensional compressor geometry, a cost comparison between the Harmonic Balance method and the time-accurate BDF scheme showed an order of magnitude savings

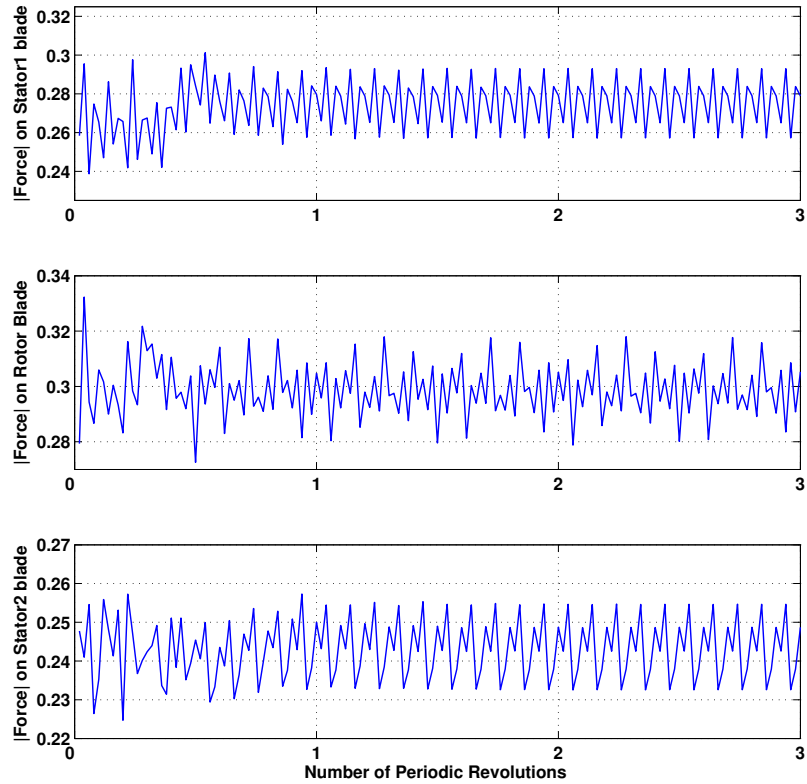
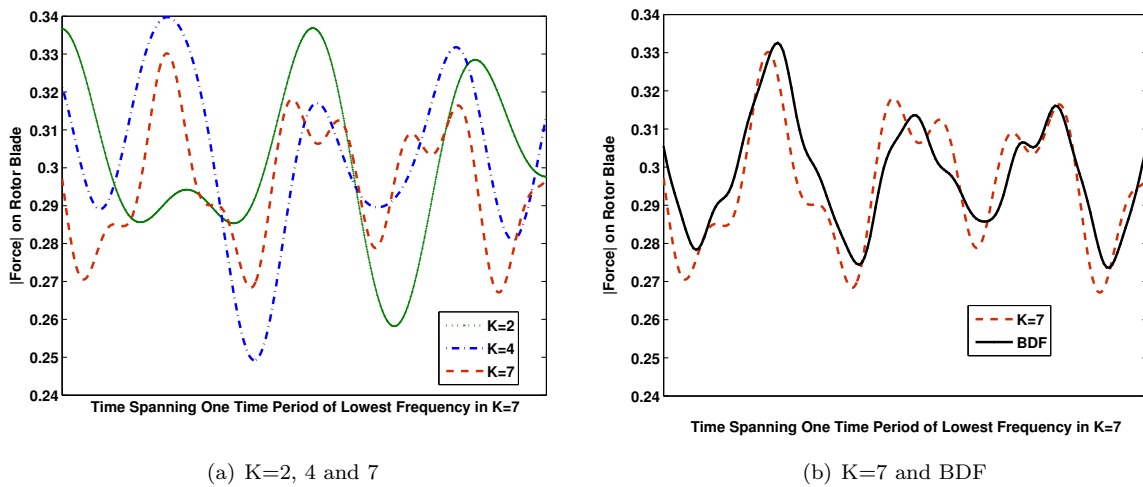


Figure 10. Configuration D using BDF: Force variation on the three blades as the BDF scheme resolves transients to reach periodic state(Plotted once every 25 physical time steps)



(a) K=2, 4 and 7

(b) K=7 and BDF

Figure 11. Configuration D using BDF and HB: Force variation on the rotor computed using the BDF scheme and compared with the HB computations using various frequency sets.

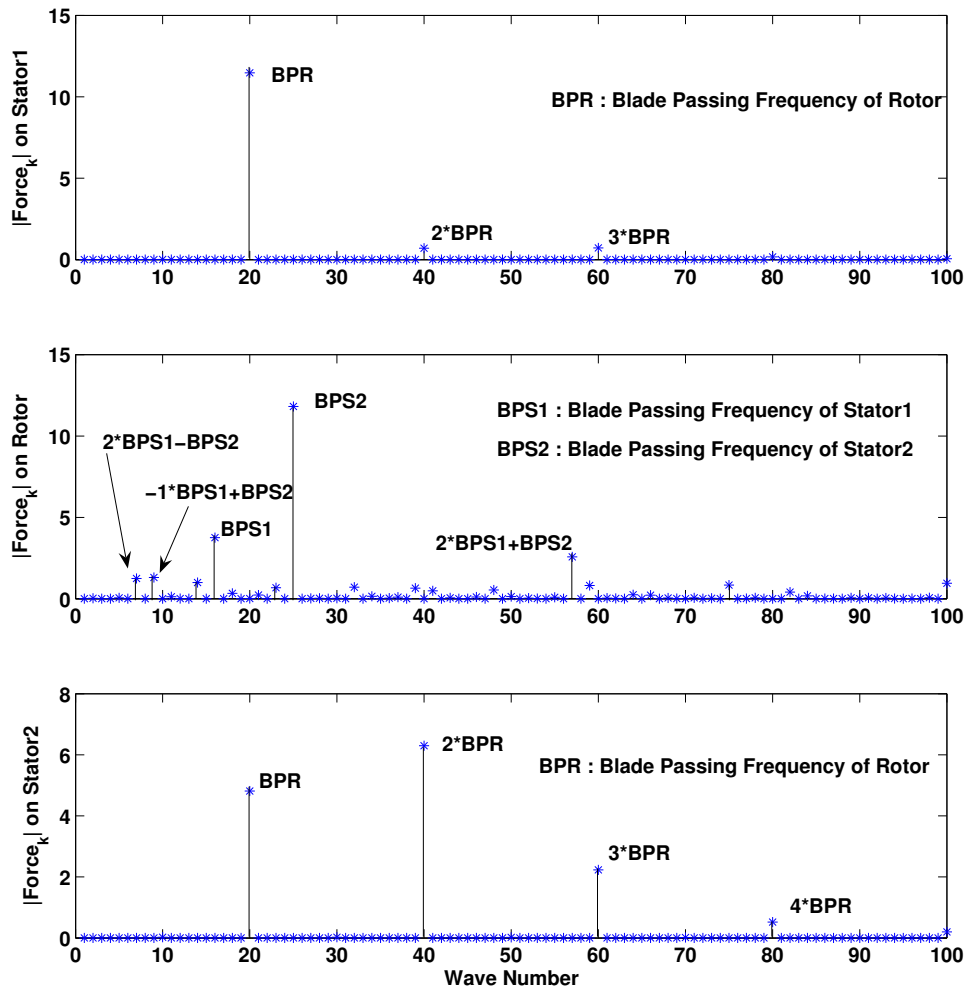


Figure 12. Configuration D using BDF: Frequency content of the force once it has reached periodic state.

in CPU requirements. Estimates from a viscous calculation on the NASA Stage 35 compressor case yield two orders of magnitude savings for the Harmonic Balance method in comparison with a BDF solution. For more complicated test cases with many more stages and more severe unsteady effects, the Harmonic Balance technique promises higher savings.

We have shown results for a two-dimensional Euler case characterised by multiple excitation frequencies and a three-dimensional RANS case using a single excitation frequency. Both these cases have looked at acoustic and wake interaction effects. In the future, combinations of frequencies from blade passing, wake interaction and/or aeroelastic deformation could be studied. Both the test cases in this paper, have had only immediate neighbors. It would also be interesting to study the effect of blade passing of a distant neighbor, since a practical turbomachine almost always has many stages and such interaction sometimes occur (although they are not always significant). The current implementation of the algorithm can be used as is, since only the appropriate frequency sets need to be specified.

As the number of stages is increased, a reduced order model like the one we have proposed would not be well suited if a very high fidelity solution is sought, unless a very large number of frequencies are resolved. In such a case, a quick calculation can be done where only the immediate neighbor's blade passing frequencies are resolved. This solution could then be provided as an initial guess to a time-accurate method so that a high quality periodic solution can be obtained much faster.

V. ACKNOWLEDGMENT

This work has benefited from the generous support of the Department of Energy under contract number LLNL B341491 as part of the Advanced Simulation and Computing Program (ASC) program at Stanford University. The authors would like to thank Dr. Dale VanZante, Dr. Anthony J. Strazisar and Dr. Russel W. Claus from the NASA Glenn Research Center for providing us the Stage 35 geometry. We would also like to thank Mr. San Gunawardana from Stanford University for helping us grid the geometry.

References

- ¹J. Yao, A. Jameson, J.J. Alonso, and F. Liu. Development and validation of a massively parallel flow solver for turbomachinery flows. *AIAA Paper 00-0882*, 38th Aerospace Sciences Meeting and Exhibit, June 2000.
- ²J. Yao, R.L. Davis, J.J. Alonso, and A. Jameson. Unsteady flow investigations in an axial turbine using the massively parallel flow solver tfo. *AIAA Paper 01-0529*, 39th Aerospace Sciences Meeting and Exhibit, June 2001.
- ³J. Yao, A. Jameson, J.J. Alonso, and F. Liu. Development and validation of a massively parallel flow solver for turbomachinery flows. *Journal of Propulsion and Power*, 17(3):659–668, May 2001.
- ⁴A. Jameson. Time dependent calculations using multigrid, with applications to unsteady flows past airfoils and wings. (91-1596), June 1998.
- ⁵E. Van der Weide, A. Gopinath, and A. Jameson. Turbomachinery applications with the time spectral method. *AIAA paper 05-4905*, 17th AIAA Computational Fluid Dynamics Conference, Toronto, Ontario, June 6-9 2005.
- ⁶J.M. Verdon and J.R. Casper. A linearized unsteady aerodynamic analysis for transonic cascades. *J. Fluid Mechanics*, 149:403–429, 1983.
- ⁷K.C. Hall, W.S. Clark, and C.B.Lorence. A linearized euler analysis of unsteady transonic flows in turbomachinery. *ASME J. Turbomachinery*, 116(3), 1994.
- ⁸W. Ning and L. He. Computation of unsteady flows around oscillating blades using linear and nonlinear harmonic euler methods. *ASME J. Turbomachinery*, 120(3):508–514, 1998.
- ⁹L. He and W. Ning. Efficient approach for analysis of unsteady viscous flows in turbomachines. *AIAA J.*, 36(11):2005–2012, 1998.
- ¹⁰J.D. Denton and U.K. Singh. Time marching methods for turbomachinery flows. In *VKI LS 1979-07*, 1979.
- ¹¹J.I. Erdos, E. Alzner, and W. McNally. Numerical solution of periodic transonic flow through a fan stage. *AIAA Journal*, 15(11), 1997.
- ¹²M.B. Giles. Calculation of unsteady wake rotor interaction. *AIAA Journal of Propulsion and Power*, 4(4):356–362, 1998.
- ¹³L. He. An euler solution for unsteady flows around oscillating blade. *ASME J. Turbomachinery*, 112(4):714–722, 1990.
- ¹⁴L. He. A method of simulating unsteady turbomachinery flows with multiple perturbations. *AIAA J.*, 20(12), 1992.
- ¹⁵J.P. Chen and J.W. Barter. Comparison of time-accurate calculations for the unsteady interactions in turbomachinery stage. *AIAA 98-3292*, July 1998.
- ¹⁶K. Ekici and K.C. Hall. Nonlinear analysis of unsteady flows in multistage turbomachines using the harmonic balance technique. *AIAA paper 06-0422*, AIAA 44th Aerospace Sciences Meeting and Exhibit, Reno, NV, January 9-12 2006.
- ¹⁷K.C. Hall, J.P. Thomas, and W.S. Clark. Computation of unsteady nonlinear flows in cascades using a harmonic balance technique. *AIAA Journal*, 40(5):879–886, May 2002.
- ¹⁸K.C. Hall, C.B. Lorence, and W.S. Clark. Nonreflecting boundary conditions for linearized unsteady aerodynamic calculations. *AIAA Paper 93-0882*, 31st Aerospace Sciences Meeting and Exhibit, Reno, NV, January 11-14 1993.

- ¹⁹K.C. Hall and K. Ekici. Multistage coupling for unsteady flows in turbomachinery. *AIAA J.*, 43(3), March 2005.
- ²⁰J.U. Schlüter and H. Pitsch. Antialiasing filters for coupled reynolds-averaged/large -eddy simulations. *AIAA J.*, 43(3), March 2005.
- ²¹A. Gopinath and A. Jameson. Time spectral method for periodic unsteady computations over two- and three-dimensional bodies. *AIAA paper 05-1220*, AIAA 43rd Aerospace Sciences Meeting and Exhibit, Reno, NV, January 10-13 2005.
- ²²A. Gopinath and A. Jameson. Application of the time spectral method to periodic unsteady vortex shedding. *AIAA paper 06-0449*, AIAA 44th Aerospace Sciences Meeting and Exhibit, Reno, NV, January 9-12 2006.
- ²³C.E. Shannon. Communication in the presence of noise. *Proceedings of the IRE*, 37(1):10–21, January 1949.
- ²⁴S.A. Orszag. On the elimination of aliasing in finite difference schemes by filtering high-wavenumber components. *Journal of the Atmospheric Sciences*, 1074(28), 1971.
- ²⁵Annual asc report. <http://cits.stanford.edu>.
- ²⁶A. Jameson, W. Schmidt, and E. Turkel. Numerical solution of the euler equations by finite volume methods using runge kutta time stepping schemes. 1981. AIAA paper 81-1259.
- ²⁷P.R. Spalart and S.R. Allmaras. A one-equation turbulence model for aerodynamic flows. *La Recherche Aerospatiale*, 1:1–23.
- ²⁸G. Kalitzin. An efficient and robust algorithm for the solution of the v2-f turbulence model with application to turbomachinery flow. In *WEHSFF 2002 Conference*, Marseille, April 2002.
- ²⁹L. Reed and R.D. Moore. Performance of single-stage axial-flow transonic compressor with rotor and stator aspect ratios of 1.19 and 1.26, and with design pressure ratio of 1.82. Technical report, NASA, 1978. TP 1338.